Phys. Med. Biol. **45** (2000) 2619–2638. Printed in the UK PII: S0031-9155(00)08967-3

Factor analysis with *a priori* knowledge—application in dynamic cardiac SPECT

A Sitek, E V R Di Bella and G T Gullberg

Medical Imaging Research Laboratory, Department of Radiology, University of Utah, CAMT, 729 Arapeen Drive, Salt Lake City, UT 84108-1218, USA

E-mail: sarkadiu@doug.med.utah.edu

Received 26 October 1999, in final form 17 April 2000

Abstract. Two factor analysis of dynamic structures (FADS) methods for the extraction of time–activity curves (TACs) from cardiac dynamic SPECT data sequences were investigated. One method was based on a least squares (LS) approach which was subject to positivity constraints. The other method was the well known apex-seeking (AS) method. A post-processing step utilizing *a priori* information was employed to correct for the non-uniqueness of the FADS solution. These methods were used to extract ^{99m}Tc-teboroxime TACs from computer simulations and from experimental canine and patient studies. In computer simulations, the LS and AS methods, which are completely different algorithms, yielded very similar and accurate results after application of the correction for non-uniqueness. FADS-obtained blood curves correlated well with curves derived from region of interest (ROI) measurements in the experimental studies. The results indicate that the factor analysis techniques can be used for semi-automatic estimation of activity curves derived from cardiac dynamic SPECT images, and that they can be used for separation of physiologically different regions in dynamic cardiac SPECT studies.

1. Introduction

When performing functional imaging with SPECT or PET, compartmental model parameters can be estimated from blood and tissue time–activity curves (TACs). The tissue curves are often obtained from user-drawn region of interest (ROI) measurements in the reconstructed tomographic images. The blood curves are typically obtained through blood sampling or, as with tissue curves, by drawing ROIs. For cardiac imaging, use of regions in the left ventricle blood pool and in the myocardial tissue have been shown to produce good results with the single photon emitter ^{99m}Tc-teboroxime (Chiao *et al* 1994, Smith *et al* 1994, 1996). The ROI methods are generally more convenient than blood sampling but require skilful selection of appropriate regions. The ROI methods may also have reliability and reproducibility problems due to the high noise levels and poor resolution that characterize SPECT images. Several researchers have sought accurate, simple, operator independent methods, such as factor analysis, for extracting TACs (Barber 1980, Cavailloles *et al* 1984).

Factor analysis of dynamic structures (FADS) (Barber 1980, Di Paola *et al* 1982, Buvat *et al* 1993) is a semi-automatic technique used for the extraction of TACs from a series of dynamic images. FADS has advantages over the ROI technique in that it can be used to achieve reproducible results. In cardiac SPECT imaging, the TACs obtained from ROI measurements may be composites of activities from different overlapping components in the selected ROI. In SPECT, overlapping occurs due to scatter and partial volume effects. To reduce these effects the

operator must choose small ROIs which appear to be in the region of pure blood or pure tissue. This is not an easy task due to the high noise levels present in dynamic images, and requires a significant amount of time to carefully choose of the order of 30 regions per cardiac study. Also, small regions used for ROI measurements will cause high noise levels in the resulting ROI TACs. In contrast, FADS methods can separate partially overlapping regions that have different temporal behaviours (Nijran and Barber 1985, Nakamura *et al* 1989, Houston and Sampson 1997). For example, Wu *et al* (1995) successfully extracted the blood TACs from dynamic cardiac PET FDG studies. FADS can also separate different physiological regions and automatically define regions in the image that have the highest concentrations of blood or tissue components. In the work presented here, it is shown that FADS can be used to separate the blood pools and myocardial tissue regions in dynamic ^{99m}Tc-teboroxime SPECT images. This method can also be used as an aid for better determination of the regions of interest in the ROI technique (Pedersen *et al* 1994).

Usually, the FADS procedure is used first to determine the low-dimensional *study sub-space* in which most of the vectors representing the evolution in time for each voxel are contained. The dimensionality of the study space is equal to the number of dynamic components in the image. This is ordinarily done by performing an orthogonal analysis of the data. As a result of orthogonal analysis the study subspace is spanned by a set of orthogonal basis vectors. The next step is oblique rotation, which provides a new set of non-orthogonal and non-negative basis vectors (*factors*). The oblique rotation also imposes non-negativity on the coordinates of the vectors which represent the data. These coordinates are also called the *factor coefficients*. Factor coefficients are simply the images of a given factor. Although there is evidence that this procedure gives reasonable results, FADS with non-negativity constraints are not quantitative due to the non-uniqueness of the FADS solution (Houston 1984). This means that there can be many different solutions which satisfy positivity constraints yet the solutions can be distinctly different depending on the method used to extract factors and factor coefficients. In order to improve quantitation of the solution of FADS, *a priori* physiological information can be used (Nijran and Barber 1986).

The goal behind this work was to develop a semi-automatic method for the extraction of TACs from dynamic cardiac SPECT sequences. Two FADS methods were employed—one the 'standard' FADS of Di Paola *et al* (1982), and the other a more direct approach that will be developed in this paper. Both used *a priori* knowledge about the heart physiology and uptake characteristics of teboroxime. FADS methods were employed and tested first with computer simulations, and then used for experimental cardiac ^{99m}Tc-teboroxime canine and patient studies.

2. Theory

2.1. Least squares factor analysis of dynamic structures (LS-FADS)

The fundamental assumption behind factor analysis methods is that changes in pixel intensities over time can be described as a linear combination of factors $\tilde{\mathbf{F}}$, where the coefficients of the combination are defined in $\tilde{\mathbf{C}}$. Thus, the factor model is expressed by

$$\mathbf{A} = \tilde{\mathbf{C}}\tilde{\mathbf{F}} + \varepsilon \tag{1}$$

where $\mathbf{A}$ is the matrix of measured data of size $N \times M$, with N being the number of pixels in one image and M the number of time frames; $\tilde{\mathbf{C}}$ contains factor coefficients for each pixel and $\tilde{\mathbf{F}}$ is a $K \times M$ matrix of time activity curves (TACs). Matrix $\tilde{\mathbf{C}}$ is $N \times K$ with K being the number of factors. ε is a random error term. The usual approach for finding $\tilde{\mathbf{C}}$ and $\tilde{\mathbf{F}}$, which

is the goal of FADS, is to perform a singular value decomposition (SVD) of preprocessed data and then to impose non-negativity constraints on the SVD solution (Di Paola *et al* 1982, Nakamura *et al* 1989, Sitek *et al* 1999a).

In this paper we propose a least squares (LS) approach. In the LS method, the singular value decomposition is not required. Assuming the factor model expressed by (1), a χ^2 function is minimized under positivity constraints imposed by an additional term in the objective function. This method requires an initial estimation of the number of factors. The total objective function is a Cartesian norm between the data and the model modified by non-negativity constraints and is given by

$$f(\mathbf{C}, \mathbf{F}) = \sum_{\substack{n=1 \\ m=1}}^{N,M} (A_{n,m} - (\mathbf{CF})_{n,m})^2 + f_{\text{nneg}}(\mathbf{C}, \mathbf{F}) \tag{2}$$

where f_{nneg} imposes non-negativity and is defined as

$$f_{\text{nneg}}(\mathbf{C}, \mathbf{F}) = \sum_{\substack{n=1 \\ k=1}}^{N,K} s_C C_{n,k}^2 H(C_{n,k}) + \sum_{\substack{k=1 \\ m=1}}^{K,M} s_F F_{k,m}^2 H(F_{k,m}) \tag{3}$$

where s_C and s_F are constants defining the 'strength' of the non-negativity constraints in the objective function, and $H(x)$ is

$$H(x) = \begin{cases} 1 & \text{if } x < 0 \\ 0 & \text{if } x \geqslant 0. \end{cases} \tag{4}$$

Matrices $\mathbf{C}$ and $\mathbf{F}$ represent estimates of true physiological matrices $\tilde{\mathbf{C}}$ and $\tilde{\mathbf{F}}$. However, the estimates may differ from the truth for three reasons. First, they may differ due to noise which exists in $\mathbf{A}$ in (1), but is not modelled in the objective function. Second, the assumed factor model may not accurately represent the physiology. Third, FADS with a non-negativity constraint gives a solution that is not necessarily unique.

2.2. Correction for non-unique solution

We found that the non-uniqueness of FADS was the main source of error when FADS was used for analysis of teboroxime cardiac images (Sitek *et al* 1999a). In this paper a post-processing technique using *a priori* information was used to correct for the non-uniqueness of the FADS solution (Sitek *et al* 1999b). This technique is specifically designed for cardiac imaging. The derivation of the correction consists of three main steps. First, it will be proved that factors and factor coefficients found by FADS with non-negativity constraints are the linear combinations of the true factors and true factor coefficients as long as the number of components is chosen appropriately. Second, the coefficients of these linear combinations (*contamination coefficients*) will be considered in the light of certain *a priori* assumptions about the true factors: (a) true factor coefficients do not completely overlap, (b) there is a time delay between the LV and RV (the RV component appears earlier in the image) and (c) there is a time delay between the tissue and the LV and RV factors. These *a priori* assumptions will lead to a conclusion that some of the contamination coefficients will have to be equal to zero, and the rest of them will be shown to be either greater or less than zero. Third, the values of constrained but still unknown contamination coefficients will be found using the following *a priori* knowledge.

(a) The value of the tissue factor coefficient inside the LV should be zero.
(b) The value of the tissue factor coefficient inside the RV should be zero.

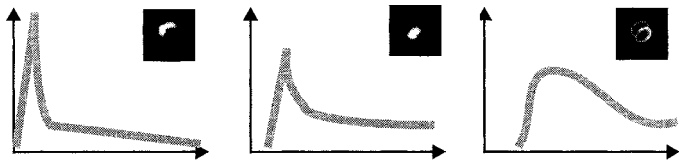

Figure 1. Schematic factors (curves) and factor coefficients (images) for cardiac teboroxime imaging with three components. From left: RV, LV and tissue.

(c) The value of the LV factor coefficient inside the RV should be zero.

(d) The value of the RV factor coefficient inside the LV should be zero.

2.2.1. Proof of linear dependence. Considering the matrix **F** as a set of M-dimensional row vectors, and the matrix **C** as a set of N-dimensional column vectors, the main assumption behind the correction for non-uniqueness is that the set of factors **F** acquired by non-unique FADS is a linear combination of the true $\tilde{\mathbf{F}}$, and that the factor coefficient vectors **C** are linear combinations of the true $\tilde{\mathbf{C}}$, and vice versa. Saying this differently K M-dimensional row vectors **F** span the same K-dimensional vector space Ω_F as the vector space $\Omega_{\tilde{F}}$ spanned by the row vectors of $\tilde{\mathbf{F}}$, and K N-dimensional column vectors **C** span the same K-dimensional vector space Ω_C as the vector space spanned by the column vectors of $\tilde{\mathbf{C}}$. The above equality is guaranteed by the equation

$$\mathbf{CF} = \tilde{\mathbf{C}}\tilde{\mathbf{F}} \tag{5}$$

because it follows from (5) that $\mathbf{F} = [(\mathbf{C}^{\mathrm{T}}\mathbf{C})^{-1}\mathbf{C}^{\mathrm{T}}\tilde{\mathbf{C}}]\tilde{\mathbf{F}}$, thus the vectors **F** are linear combinations of $\tilde{\mathbf{F}}$, so Ω_F is a subspace of $\Omega_{\tilde{F}}$. By transforming (5) into $\tilde{\mathbf{F}} = [(\tilde{\mathbf{C}}^{\mathrm{T}}\tilde{\mathbf{C}})^{-1}\tilde{\mathbf{C}}^{\mathrm{T}}\tilde{\mathbf{C}}]\mathbf{F}$ it can be concluded also that $\Omega_{\tilde{F}}$ is a subspace of Ω_F, so $\Omega_{\tilde{F}} = \Omega_F$ must hold. Similarly, from (5) it can be shown that $\Omega_{\tilde{C}} = \Omega_C$.

2.2.2. Derivation of the matrix contamination coefficients. For cardiac imaging, schematically presented in figure 1, the image of the healthy heart consists of three factors: right ventricle (RV) blood pool, left ventricle (LV) blood pool and myocardial tissue. In general, factors acquired by FADS with only the non-negativity constraints in the case of heart imaging are linear combinations of true factors, as was shown in section 2.2.1:

$$\begin{aligned}
\boldsymbol{F}_R &= 1\,\tilde{\boldsymbol{F}}_R - x_{RL}\tilde{\boldsymbol{F}}_L - x_{RT}\tilde{\boldsymbol{F}}_T \\
\boldsymbol{F}_L &= 1\,\tilde{\boldsymbol{F}}_L - x_{LR}\tilde{\boldsymbol{F}}_R - x_{LT}\tilde{\boldsymbol{F}}_T \\
\boldsymbol{F}_T &= 1\,\tilde{\boldsymbol{F}}_T - x_{TR}\tilde{\boldsymbol{F}}_R - x_{TL}\tilde{\boldsymbol{F}}_L
\end{aligned} \tag{6}$$

where $\boldsymbol{F}_R$, $\boldsymbol{F}_L$ and $\boldsymbol{F}_T$ are factor row vectors obtained by FADS with non-negativity constraints, $\tilde{\boldsymbol{F}}_R$, $\tilde{\boldsymbol{F}}_L$ and $\tilde{\boldsymbol{F}}_T$ are the true factors of RV, LV and tissue and $x_{RL}, \ldots$ are the contamination coefficients. Generality is not lost by fixing some of the contamination factors in (6) to 1, because the normalization of the true factors $\tilde{\boldsymbol{F}}_R$, $\tilde{\boldsymbol{F}}_L$ and $\tilde{\boldsymbol{F}}_T$ has not yet been specified. Therefore, (6) requires implicit normalization of the true factors in order that (6) holds. It has been reported in the literature that FADS with non-negativity constraints give curves which resemble true factors, suggesting that the constants $x_{RL}, \ldots$ in (6) are much smaller than 1. We also have found that the maximum values of $x_{RL}, \ldots$ in (6) are of the order of 0.1. Value of the contamination coefficient x_{RL} can be interpreted as LV blood factor contamination in the

RV blood factor and other contamination coefficients can be interpreted likewise. In matrix notation (6) can be expressed as

$$\begin{bmatrix} \boldsymbol{F}_R \\ \boldsymbol{F}_L \\ \boldsymbol{F}_T \end{bmatrix} = \begin{bmatrix} 1 & -x_{RL} & -x_{RT} \\ -x_{LR} & 1 & -x_{LT} \\ -x_{TR} & -x_{TL} & 1 \end{bmatrix} \begin{bmatrix} \tilde{\boldsymbol{F}}_R \\ \tilde{\boldsymbol{F}}_L \\ \tilde{\boldsymbol{F}}_T \end{bmatrix} = \mathbf{M}\tilde{\mathbf{F}} \tag{7}$$

with $\mathbf{M}$ defined as

$$\mathbf{M} := \begin{bmatrix} 1 & -x_{RL} & -x_{RT} \\ -x_{LR} & 1 & -x_{LT} \\ -x_{TR} & -x_{TL} & 1 \end{bmatrix}. \tag{8}$$

Inverting $\mathbf{M}$ gives

$$\mathbf{M}^{-1} = \frac{1}{\det\mathbf{M}} \begin{bmatrix} 1 - x_{TL}x_{LT} & x_{RL} + x_{TL}x_{RT} & x_{RT} + x_{RL}x_{LT} \\ x_{LR} + x_{TR}x_{LT} & 1 - x_{TR}x_{RT} & x_{LT} + x_{LR}x_{RT} \\ x_{TR} + x_{LR}x_{TL} & x_{TL} + x_{TR}x_{RL} & 1 - x_{RL}x_{LR} \end{bmatrix} \tag{9}$$

and neglecting the second order terms of the constants, $x_{TL}x_{LT}, \ldots$, since the constants are small, the inverse $\mathbf{M}^{-1}$ can be expressed as

$$\mathbf{M}^{-1} \approx \begin{bmatrix} 1 & x_{RL} & x_{RT} \\ x_{LR} & 1 & x_{LT} \\ x_{TR} & x_{TL} & 1 \end{bmatrix}. \tag{10}$$

Thus, using matrix notation, it follows from (5) and (10) that

$$[\, \boldsymbol{C}_R \quad \boldsymbol{C}_L \quad \boldsymbol{C}_T \,] = \tilde{\mathbf{C}}\mathbf{M}^{-1} \approx [\, \tilde{\boldsymbol{C}}_R \quad \tilde{\boldsymbol{C}}_L \quad \tilde{\boldsymbol{C}}_T \,] \begin{bmatrix} 1 & x_{RL} & x_{RT} \\ x_{LR} & 1 & x_{LT} \\ x_{TR} & x_{TL} & 1 \end{bmatrix}. \tag{11}$$

Considering (7) and the fact that $\mathbf{F}$ was found under non-negativity constraints the true RV factor cannot be subtracted from the true tissue factor since the activity in the tissue is delayed with respect to RV (figure 1). Such subtraction would create negative values in the estimated tissue factor. Since the subtraction is not allowed, the corresponding coefficient in (7), $-x_{TR}$, must be larger than or equal to zero if the non-negativity of the $\boldsymbol{F}_T$ factor is to hold. Similarly it can be shown that $-x_{LR} \geqslant 0$.

However, it can also be noticed in figure 1 that from the true RV factor certain amounts of the true LV and true tissue factors can be subtracted without violating the non-negativity constraints of the RV factor. Therefore, using there considerations no constraints can be put on the values of $-x_{RL}$ and $-x_{RT}$. Also the true tissue factor can be subtracted from the true LV factor without violating non-negativity of the factors obtained by FADS with non-negativity constraints. In summary: the non-negativity of $\mathbf{F}$ puts the following constraints on the contamination coefficients: $-x_{TR} \geqslant 0$ and $-x_{LR} \geqslant 0$.

Now consider the assumption (a) made in section 2.2 that the true factor coefficients do not completely overlap. If even a single pixel of each component is 'pure' then the subtraction of the non-zero factor coefficient at that location from the factor coefficients of the other components will result in negatives on the left-hand side of (11). Since a non-negativity constraint was used to find the left-hand side of (11), it is clear that all of the contamination coefficients in (11) must be greater than or equal to zero.

However, this assumption fails to consider that approximately 10–20% of the volume of a tissue region consists of capillaries carrying blood. That is, the (LV) blood pool coefficient completely underlays the tissue coefficient image. Thus, some of the true tissue factor coefficient image can be subtracted from the LV blood coefficient image without violating the non-negativity constraint, which implies that x_{TL} does not have to be greater than zero.

These considerations lead to the following: $x_{TR} \geqslant 0, x_{RL} \geqslant 0, x_{RT} \geqslant 0$ and $x_{LR} \geqslant 0$. Combining these conditions with the previous ones gives the following constraints on the contamination coefficients: $x_{LR} = 0, x_{TR} = 0, x_{RL} \geqslant 0, x_{RT} \geqslant 0$ and $x_{LT} \geqslant 0$, so the general form of (7) can be rewritten

$$\begin{bmatrix} \boldsymbol{F}_R \\ \boldsymbol{F}_L \\ \boldsymbol{F}_T \end{bmatrix} = \begin{bmatrix} 1 & -x_{RL} & -x_{RT} \\ 0 & 1 & -x_{LT} \\ 0 & -x_{TL} & 1 \end{bmatrix} \begin{bmatrix} \tilde{\boldsymbol{F}}_R \\ \tilde{\boldsymbol{F}}_L \\ \tilde{\boldsymbol{F}}_T \end{bmatrix} = \mathbf{M}\tilde{\mathbf{F}} \tag{12}$$

and the corresponding form of (11) is

$$[\, \boldsymbol{C}_R \quad \boldsymbol{C}_L \quad \boldsymbol{C}_T \,] = \tilde{\mathbf{C}}\mathbf{M}^{-1} \approx [\, \tilde{\boldsymbol{C}}_R \quad \tilde{\boldsymbol{C}}_L \quad \tilde{\boldsymbol{C}}_T \,] \begin{bmatrix} 1 & x_{RL} & x_{RT} \\ 0 & 1 & x_{LT} \\ 0 & x_{TL} & 1 \end{bmatrix}. \tag{13}$$

2.2.3. Estimation of contamination coefficients. In order to find unknown coefficients $x_{RL}, \ldots$ in (12) and (13) *a priori* knowledge (a)–(d) listed at beginning of section 2.2 was used. Equation (13) can alternatively be written as

$$\begin{aligned} \boldsymbol{C}_R &\approx \tilde{\boldsymbol{C}}_R \\ \boldsymbol{C}_L &\approx x_{RL}\tilde{\boldsymbol{C}}_R + \tilde{\boldsymbol{C}}_L + x_{TL}\tilde{\boldsymbol{C}}_T \\ \boldsymbol{C}_T &\approx x_{RT}\tilde{\boldsymbol{C}}_R + x_{LT}\tilde{\boldsymbol{C}}_L + \tilde{\boldsymbol{C}}_T. \end{aligned} \tag{14}$$

It can be seen from (14) that $\tilde{\boldsymbol{C}}_R \approx \boldsymbol{C}_R$, so that non-negativity constraints give a unique RV coefficient image. To find values of $x_{RL}, \ldots$, consider the average value of the factor coefficients for pixels corresponding to the RV. These pixels are defined as pixels with the highest value in the image RV coefficient $\boldsymbol{C}_R$. In this paper the three pixels with the highest value of the given factor coefficients were always used. Let the notation $\boldsymbol{C}_R$(LV) denote the average value of the RV coefficient of the three pixels which have the highest values of LV coefficient and similarly for others. Using this notation the *a priori* conditions (a)–(d) can be listed as

$$\begin{aligned} &\text{(a) } \tilde{\boldsymbol{C}}_T(\text{LV}) = 0 \\ &\text{(b) } \tilde{\boldsymbol{C}}_T(\text{RV}) = 0 \\ &\text{(c) } \tilde{\boldsymbol{C}}_L(\text{RV}) = 0 \\ &\text{(d) } \tilde{\boldsymbol{C}}_R(\text{LV}) = 0. \end{aligned} \tag{15}$$

Considering the first and the second equations in (14) and evaluating the average values of the factor coefficients for the RV we have that $x_{RL} = \boldsymbol{C}_L(\text{RV})/\boldsymbol{C}_R(\text{RV})$. Similarly other coefficients can be found (please see the appendix for the complete derivation of (16)) to give the following results:

$$\begin{aligned} x_{RL} &= \frac{\boldsymbol{C}_L(\text{RV})}{\boldsymbol{C}_R(\text{RV})} \\ x_{RT} &= \frac{\boldsymbol{C}_T(\text{RV})}{\boldsymbol{C}_R(\text{RV})} \\ x_{LT} &= \frac{\boldsymbol{C}_T(\text{LV})}{\boldsymbol{C}_L(\text{LV})}. \end{aligned} \tag{16}$$

Using these considerations only the value of x_{TL} cannot be found because the tissue component is completely overlapped by the LV (see the appendix). Knowing the values of the

contamination coefficients from (16), true factors can be found by inverting (12) and true factor coefficients by inverting (13):

$$\begin{bmatrix} \tilde{\boldsymbol{F}}_R \\ \tilde{\boldsymbol{F}}_L \\ \tilde{\boldsymbol{F}}_T \end{bmatrix} = \mathbf{M}^{-1}\mathbf{F} \approx \begin{bmatrix} 1 & x_{RL} & x_{RT} \\ 0 & 1 & x_{LT} \\ 0 & x_{TL} & 1 \end{bmatrix} \begin{bmatrix} \boldsymbol{F}_R \\ \boldsymbol{F}_L \\ \boldsymbol{F}_T \end{bmatrix} \tag{17}$$

and true coefficients

$$[\,\tilde{\boldsymbol{C}}_R \quad \tilde{\boldsymbol{C}}_L \quad \tilde{\boldsymbol{C}}_T\,] = \mathbf{CM} = [\,\boldsymbol{C}_R \quad \boldsymbol{C}_L \quad \boldsymbol{C}_T\,] \begin{bmatrix} 1 & -x_{RL} & -x_{RT} \\ 0 & 1 & -x_{LT} \\ 0 & -x_{TL} & 1 \end{bmatrix}. \tag{18}$$

The lack of knowledge of the value of x_{TL} leaves the tissue curve biased by the LV curve in (17), and biases the LV image coefficient by the tissue coefficient image in (18).

Equations (16)–(18) provide a procedure for correcting the FADS solution for the case of teboroxime cardiac imaging.

3. Methods

Two FADS methods were studied in this paper. The method described in section 2.1 will be referred to as the least squares method (LS method). This method requires non-linear minimization. The objective function (2) was minimized by the conjugate gradient algorithm (Press *et al* 1996). In order to compare the non-standard LS FADS method to an established technique, results from the apex-seeking method (Di Paola *et al* 1982) are presented alongside the results of the LS FADS method from computer simulations and from normal canine studies. The apex-seeking method will be referred to as the AS method. Results from both the LS and the AS methods were corrected for non-uniqueness by the method described in section 2.2. The corrected methods will be referred to as CLS and CAS for corrected least squares and corrected apex-seeking methods, respectively.

3.1. Computer simulations

Computer simulations were performed using the MCAT phantom (Tsui *et al* 1993). A time series of images were created from a slice of the heart region of the MCAT phantom. Each image was 64 × 64 pixels in size and each image consisted of three factors: left ventricle blood, right ventricle blood and myocardial tissue. The spatial distributions of these factors are presented in figure 2. To simulate the resolution effects there was a 1 pixel overlap between different components, i.e. there was 1 pixel overlap of the tissue (figure 2(c)) with the RV blood pool (figure 2(b)), and 1 pixel overlap of the LV tissue (figure 2(c)) with the LV blood pool (figure 2(a)). There is also an overlap between the background (figure 2(d)) and all other components. Although the assumed overlap was just 1 pixel, it is quite substantial for the tissue (figure 2(c)), which has a thickness of 1–3 pixels.

The LV blood component completely underlays the tissue and the background. This is because of the presence of the LV blood pool component in the heart tissue was assumed (see (21)). The background component is assumed to be the same as the LV component but with smaller amplitude (see the following details).

The blood activity in the LV and in the background resulting from a bolus infusion LV(t), was simulated by the function used by Smith *et al* (1996) and was of the form

$$\mathrm{LV}(t) = \begin{cases} 0 & t \leqslant 10 \\ 120(t-10)/20 & 10 < t \leqslant 30 \\ 104\mathrm{e}^{-0.1(t-30)} + 16\mathrm{e}^{-0.001(t-30)} & t > 30 \end{cases} \tag{19}$$

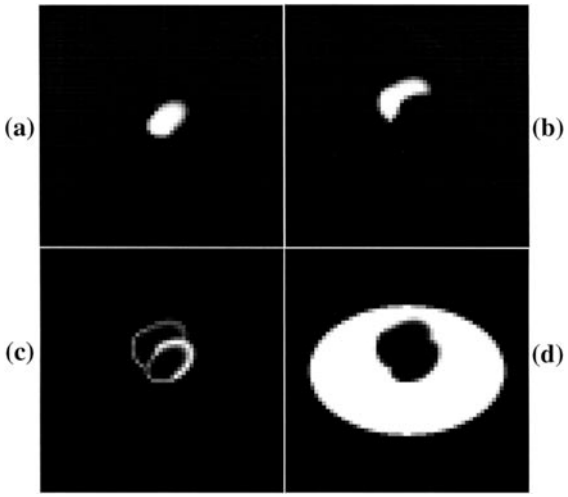

Figure 2. Images of factor coefficients used in computer simulation (MCAT phantom): (a) LV, (b) RV, (c) tissue and (d) background.

where t is the time expressed in seconds. The background activity was assumed to be one-tenth of the LV activity.

The activity in the right ventricle $\mathrm{RV}(t)$ was simulated assuming that it had a strong peak at the beginning of the study and then asymptotically approached the LV blood component. Such behaviour is consistent with results of experiments in which the bolus with the radioactive $^{99\mathrm{m}}$Tc-teboroxime goes first to the RV and then, over time, the activities in both ventricles become equal. The following function was used for the RV activity:

$$\mathrm{RV}(t) = \begin{cases} 240t/10 & t \leqslant 10 \\ 224\mathrm{e}^{-0.1(t-10)} + 16\mathrm{e}^{-0.001(t-10)} & t > 10. \end{cases} \tag{20}$$

The tissue component activity concentration $\mathrm{T}(t)$ was formed to simulate the uptake of $^{99\mathrm{m}}$Tc-teboroxime, following a two compartment model, and was calculated using the following integration:

$$\mathrm{T}(t) = k_{21} \int_0^t \mathrm{e}^{-k_{12}\tau} \mathrm{LV}(t-\tau)\,\mathrm{d}\tau + f_v \mathrm{LV}(t). \tag{21}$$

The presence of vasculature in the heart tissue was simulated by setting f_v equal to 0.15. Values of k_{12} wash-out and k_{21} wash-in were equal to 0.40 and 0.68 min^{-1}, respectively, and were chosen to represent stress conditions in the heart. One hundred and eighty-three dynamic images, each taken over 6 seconds, were simulated. Tomographic projections and reconstructions were not simulated. Data were simulated with 25% Gaussian noise, i.e. the variance was 25% of the pixel value. After adding noise, all negative values were rounded to zero. Thirty independent noise realizations were performed. A 20×19 pixel region encompassing the heart was the only region analysed. To assess the accuracy of the FADS acquired curves, the Cartesian norms between the true curves and curves obtained by all of the FADS were calculated. The kinetic wash-in parameter (k_{21}), wash-out parameter (k_{12}) and vascular fraction (f_v) were determined from the curves obtained by FADS and compared to the kinetic parameters obtained from the true curves. Kinetic parameters were estimated using RFIT (Huesman and Mazoyer 1987), and their standard deviations were calculated using 30 noise realizations.

3.2. Experimental canine studies

Data from 16 (eight at rest and eight at stress) canine studies were used to evaluate the factor analysis techniques. A three-detector scanner (PRISM 3000XP, Picker International, Inc., Cleveland, OH) with fan-beam collimators (65 cm focal length) was used to acquire transmission and emission projection data. The transmission scan was performed prior to the emission acquisition by using a ^{153}Gd fan-beam transmission line source. Without moving the dogs, a bolus of ^{99m}Tc-teboroxime was injected 5 seconds after the start of the dynamic acquisition. The camera acquired 120 projections over 360° every 6 seconds for 17 minutes. The 179 dynamic 3D images were reconstructed using 25 iterations of the ML-EM algorithm (Shepp and Vardi 1982) with attenuation correction using attenuation maps that were determined by the transmission scan and scaled to the energy of ^{99m}Tc. The acquisition protocols for the rest and stress studies were the same. The reconstructed 3D images were then reoriented to obtain short-axis slices of the heart. Both factor analysis methods were applied to an 11×11 pixel region encompassing a short-axis slice of the myocardium, with the size of the pixel equal to 0.712 cm. The sub-region was used to make sure that there were no additional components such as liver or pulmonary artery present in the image. Only one slice was analysed in all but one study included in this paper. In one study, six slices were taken together and analysed by FADS as volume data.

3.3. Patient study

A patient was scanned using the previously described three-detector system equipped with low-energy parallel hole high-resolution collimators. The transmission scan using a fan-beam collimator and a ^{153}Gd line source was performed before the emission acquisition. The values of the attenuation map were scaled to the energy of ^{99m}Tc. External ^{99m}Tc markers were used to align the transmission and emission images. The system acquired 120 64×64 pixel emission projections every 10 seconds over a 15 minute period after the injection of 614 and 1147 MBq of teboroxime for the rest and stress study, respectively. The rest and stress protocols were the same. The 90 3D dynamic images were reconstructed by employing three iterations of the OSEM algorithm (subset size six) (Hudson and Larkin 1994) with attenuation correction. FADS was applied to a sub-region of one 16×9 pixel short-axis slice of the heart region. The pixel size was 0.712 cm.

3.4. Normalization of the curves; ROI selection

The curves obtained by FADS, before and after correction for non-uniqueness, had to be scaled by an appropriate scaling factor. Determination of this scaling factor was important in order to achieve quantitative results. The scaling factors were calculated as the average value of the three highest coefficients of a given factor. Curves scaled in this way could be directly compared with ROI measurements. Wu *et al* (1995) used a similar approach to extract scaling factors, but their scaling factor was calculated from the values above a certain threshold. Houston and Sampson (1997) calculated scaling parameters in renal studies based on the total count in the factor images, which required specification of the region over which the total count was calculated. We found, based on computer simulation, that our scaling approach gave quantitatively sound results.

The ROIs used for the ROI measurements were selected based on the factor coefficient images, e.g. LV ROIs were defined by the pixels which had the highest values of LV factor coefficients. To reduce spillover effects in the ROI measurements, the chosen ROIs were small (3 pixels), and they were the same as the pixels used for the calculation of the scale factor. The

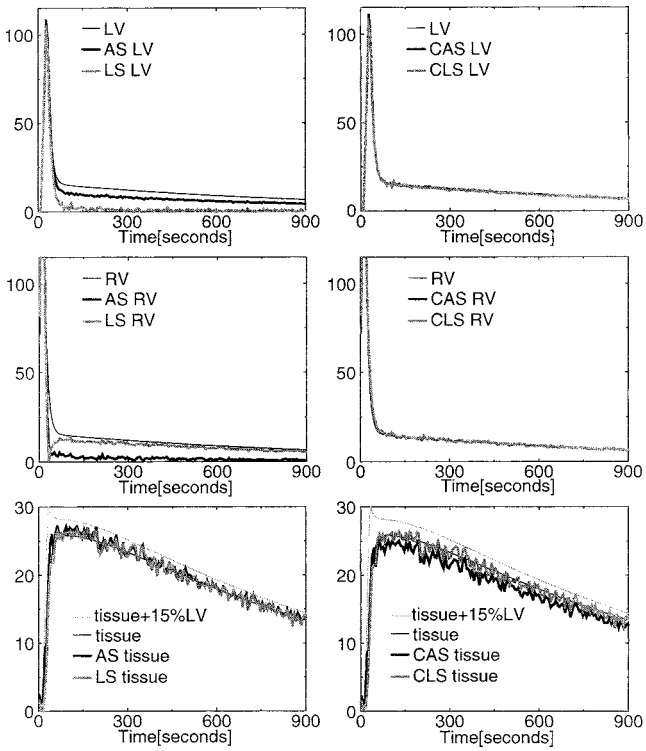

Figure 3. Results of FADS for a single noise realization of simulated teboroxime-99m uptake in the myocardium: comparison of the curves obtained by uncorrected FADS methods (AS and LS) and corrected FADS (CAS and CLS) to true curves. Rows correspond to LV, RV and myocardial tissue factors, respectively.

Table 1. Values of average curve distances with standard deviations obtained using different FADS methods.

	Curve distance			
Method	LV	RV	Tissue	Tissue+15% LV
AS	4.11 ± 0.78	9.13 ± 0.80	1.14 ± 0.40	2.52 ± 0.71
LS	9.11 ± 0.14	6.24 ± 0.80	0.78 ± 0.06	2.72 ± 0.15
CAS	0.83 ± 0.39	2.20 ± 1.18	1.22 ± 0.50	2.50 ± 0.80
CLS	0.94 ± 0.34	2.20 ± 1.19	0.85 ± 0.11	2.89 ± 0.19

ROI selection process was automatic since it used the results of the factor analysis method and did not require operator assistance.

4. Results

4.1. Factor analysis of dynamic SPECT simulation studies

Figure 3 shows the TACs obtained by different FADS methods and the comparisons to the true curves. The example presented in a single noise realization. The discrepancy between the LV and RV curves obtained by uncorrected FADS methods and the true curves is clearly visible.

Table 2. Values of kinetic parameters with standard deviations calculated from the results of different FADS methods.

	Kinetic parameters		
Method	f_v [a]	k_{12} (0.689)	k_{21} (0.405)
AS	0.003 ± 0.068	0.702 ± 0.065	0.264 ± 0.016
LS	-0.031 ± 0.012	0.672 ± 0.044	0.079 ± 0.004
CAS	0.007 ± 0.062	0.702 ± 0.060	0.415 ± 0.028
CLS	-0.031 ± 0.013	0.686 ± 0.047	0.417 ± 0.027

[a] Although the simulated value f_v was 0.15, the expected value is undetermined due to the unknown value of x_{TL} in equation (17).

After the correction is applied the agreement is improved (figure 3). The FADS methods give tissue curves which are in agreement with the pure tissue curve and agree less with the tissue curve containing an added vascular component. These findings are confirmed by the results of multiple noise realizations presented in table 1. The improvement in the LV component for the CLS method is dramatic. The final corrected results are very similar in terms of accuracy and precision for both CAS and CLS method and only the tissue curves vary substantially in precision. However, these large variations do not affect the precision of the estimated kinetic parameters k_{12} and k_{21} (table 2). These differences in tissue curves are due to a large variation in the unknown parameter x_{TL} in (17), which only affects the estimation of f_v.

Table 2 presents the kinetic parameters estimated by RFIT from the curves determined by FADS and shows kinetic parameters calculated by RFIT from noise free true curves (values in the brackets given in the caption of table 2). The estimated values of parameters k_{12} and k_{21} for CAS and CLS are very close to the values of k_{12} and k_{21} obtained by RFIT from the noiseless theoretical curves. The differences between the values of kinetic parameters obtained from noiseless curves and from curves with noise were tested with the two-tailed, paired Student's t-test (Brownlee 1965). The null hypothesis that the difference is zero can be rejected for k_{12} at the level of significance $p = 0.344$ for CAS and $p = 0.782$ for CLS methods, and it can be rejected for k_{21} with $p = 0.126$ for CAS and $p = 0.061$ for CLS methods. For the uncorrected methods, p-values are similar to those obtained by corrected methods for k_{12} (0.385 for AS and 0.100 for LS). Uncorrected AS and LS methods give a value of k_{21} which is different from the value of k_{21} obtained from noiseless curves ($p < 0.000\,001$). Values of wash-in and wash-out parameters obtained from noiseless curves are slightly different from the theoretical values which were used in generation of the curves. This difference is due to the integration and sparse temporal sampling of the curves. The negative value of the f_v parameter found in the LS study is allowed in this method because of the undetermined value of the constant x_{TL} in (17).

4.2. Factor analysis of ^{99m}Tc-teboroxime canine studies

The LS FADS analysis was applied successfully to 16 canine studies (eight at rest and eight in stress conditions) and to four patient studies (two at rest and two in stress). In this paper the results from a total of five canine and patient studies are presented, including a normal canine study, and a canine study with occlusion.

In figures 4 and 5, the results of FADS from a normal canine study are presented. Figure 4 presents the results of a canine stress study and figure 5 presents the results of a canine rest study. As in the simulation studies the correction for non-uniqueness creates better agreement between the results of the CLS and CAS methods and improves agreement

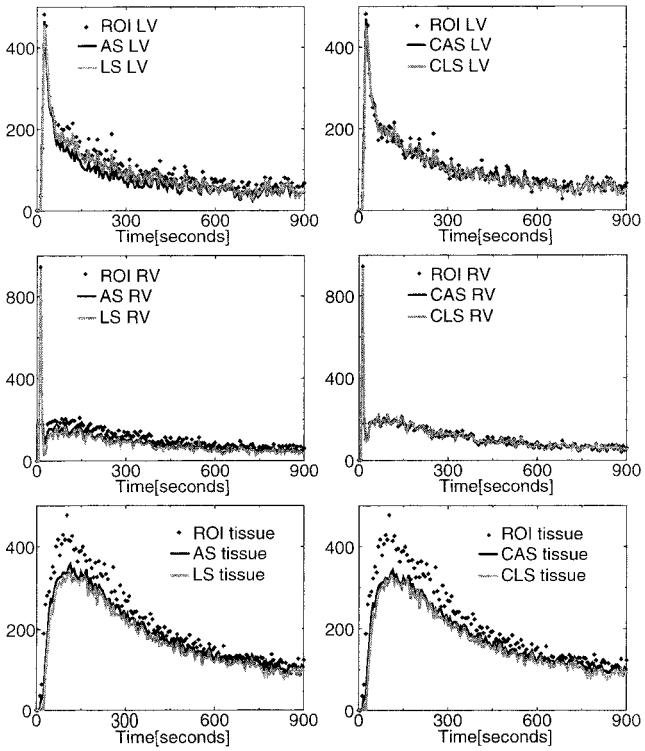

Figure 4. Results of FADS for a canine teboroxime-99m stress study: comparison of the curves obtained by uncorrected FADS methods (AS and LS) and corrected FADS methods (CAS and CLS) with curves obtained from ROI measurements. Rows correspond to LV, RV and myocardial tissue factors, respectively.

between ROI curves for the LV and RV components. There is not a strong agreement with the tissue but such agreement is not expected since, as shown in the computer simulation study, FADS separates pure tissue curves from the vascular component. Therefore, it is not surprising that ROI measurements give tissue curves different from those obtained with FADS.

The RV curve in figures 4 and 5 has a very strong peak at the beginning when the concentrated bolus reaches the RV. In the later phase of the study RV and LV components are equal. In the rest study, there is a significant discrepancy between the tissue curves obtained by the CAS method and those obtained by the CLS method, but this is probably due to the unknown x_{TL}, as was shown in a computer simulation comparing AS and LS. The rest study was performed approximately 1 hour after the stress study and there is some residual activity which elevates all of the curves for the rest study in figure 5.

Figure 6 presents images of factor coefficients for the LS results in the stress study (figures 6(a) and (b)), and the rest study (figures 6(c) and (d)). There is little difference between the corrected and uncorrected coefficients. The only noticeable difference is the increase of contrast in the image of the corrected tissue coefficient, which is particularly noticeable in the rest study, and a lessening of the contrast in the image of the LV coefficients. The image of the LV component is more spread out in the stress study. The image of the RV coefficients is larger in the rest study than it is in the stress study. There are no salient differences in the images of the myocardium between the rest study and the stress study.

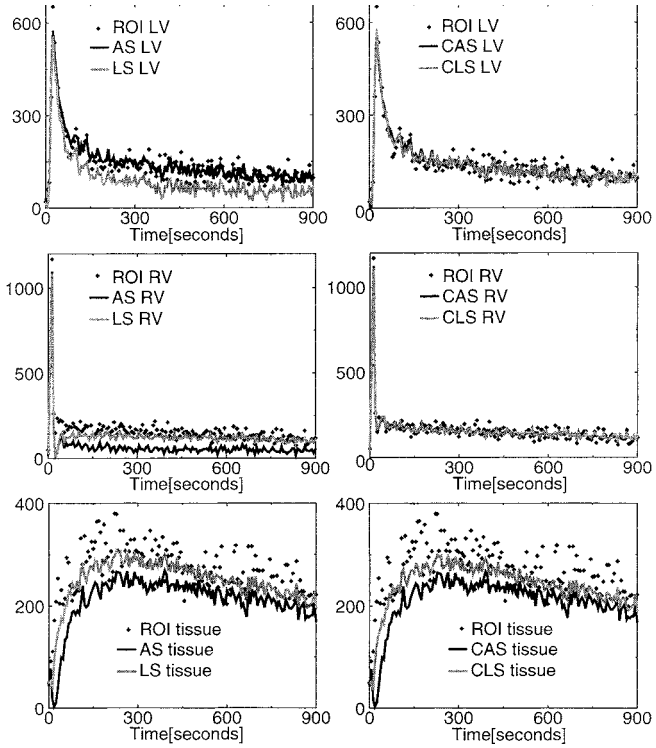

Figure 5. Results of FADS for a canine teboroxime-99m rest study: comparison of the curves obtained by uncorrected FADS methods (AS and LS) and corrected FADS methods (CAS and CLS) with curves obtained from ROI measurements. Rows correspond to LV, RV and myocardial tissue factors, respectively.

The factor analysis methods were also applied to volume data from the same canine study. Here, however, the size of the region in the analysed slices was further reduced to 7×10 pixels. The reduction was done in order to lessen the influence of the liver on the results. Because of that reduction only part of the myocardium was included in the analysis. Figure 7 shows the TACs obtained by the CLS method. For the volume data the curves are very similar to curves obtained from a one slice analysis, but the noise is less in the volume results. Figure 8 shows the corresponding factor coefficients.

4.3. Factor analysis of a ^{99m}Tc-teboroxime patient study

The TACs for the patient studies are presented in figure 9. The curves are much noisier than in the canine studies. Due to low temporal resolution (10 seconds) there is some mixing of the RV and LV components in the rest study (the RV image is non-zero in the LV). The slices in figure 10 are not perfectly co-registered since the patient was moved between the stress and rest studies. However, they do correspond to approximately the same region of the heart. As in the canine studies, the image of the coefficients of the LV is 'spread' more in the stress study than it is in the rest study. Also, the RV appears to be larger in the rest study. The image of tissue coefficients seems to be non-uniform, but it cannot be determined conclusively whether this is due to noise or from non-uniform uptake of the radio-pharmaceutical.

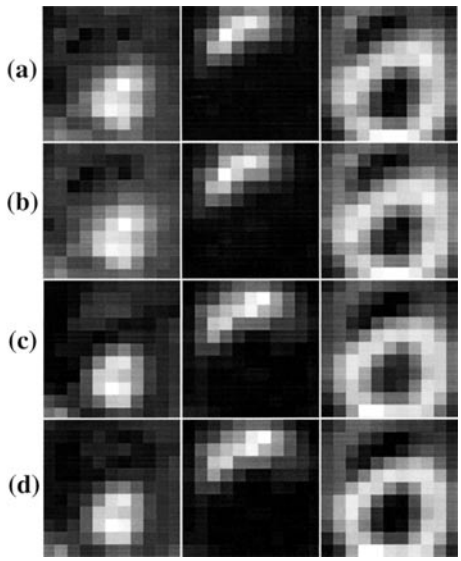

Figure 6. Images of factor coefficients obtained by the LS method, rows (a) and (c), and the CLS method, rows (b) and (d), for a teboroxime canine study. Rows (a) and (b) represent the stress study, and (c) and (d) represent the rest study. Columns from left to right correspond to LV, RV and myocardial tissue components. Factor coefficients in this figure correspond to factors presented in figures 4 and 5.

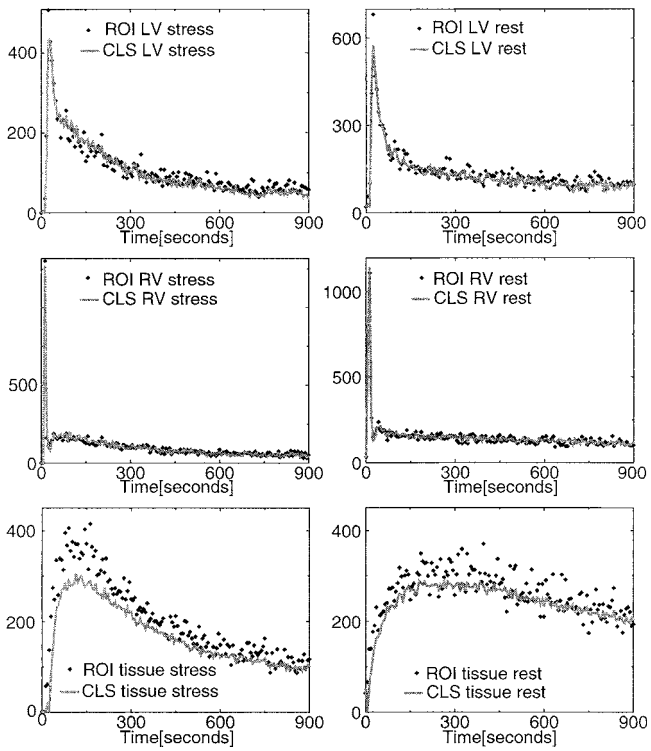

Figure 7. Results of CLS method and ROI measurements from volume (3D) data in a canine teboroxime-99m stress study (first column) and rest study (second column). Rows correspond to LV, RV and myocardial tissue components.

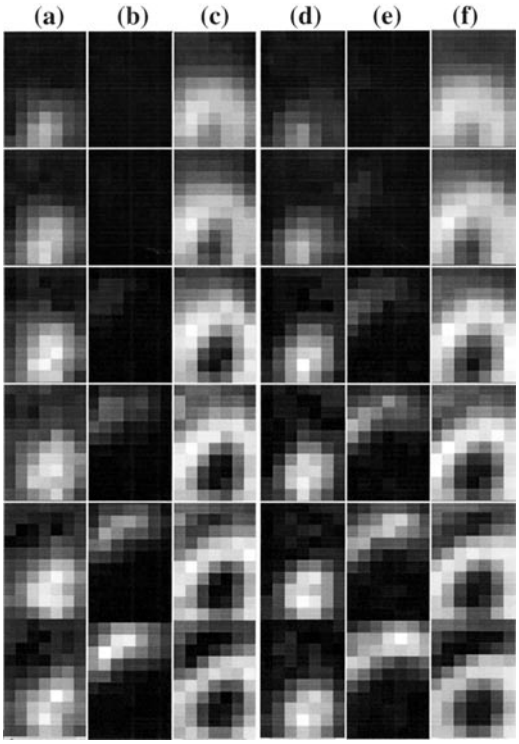

Figure 8. Images of factor coefficients obtained by the CLS method from canine volume data. Columns (a), (b) and (c) correspond to LV, RV and tissue coefficients for the stress study, and (d), (e) and (f) correspond to the rest study. Rows represent subsequent slices in the volume images of the coefficients.

5. Discussion

In this paper two factor analysis techniques were applied to dynamic cardiac SPECT imaging. The techniques enabled the estimation of the LV and RV factor curves and were used for extracting tissue curves averaged over part of the myocardium. FADS, as described in this paper, gives tissue curves that are mixed with the LV component. The authors speculate that incorporation of the two-compartment kinetic model of teboroxime uptake into the FADS algorithm may help to resolve the problem of the unknown value of x_{TL} in equation (17). The problem of the unknown x_{TL} however may not be critical, because the kinetic parameters can be estimated from tissue TACs biased by LV curves as long as LV TACs are provided correctly. More importantly, in using FADS with three components the assumption is made that the myocardium is uniform and that the uptake of the pharmaceutical occurs at the same rate through the entire volume of the myocardium. However, this is not true for abnormal regions which have dynamically different uptake.

When imaging an abnormal heart more components must be used. This is an open issue, since in a particular heart there may be regions with different amounts of infarction and ischemia and theoretically each of these regions would have a different temporal behaviour. Questions remain as to whether FADS would be able to separate all of the different regions in an abnormal myocardium given noisy SPECT data, and whether it would be possible to overcome the non-uniqueness effects for such FADS analysis. This separation would be a difficult task due

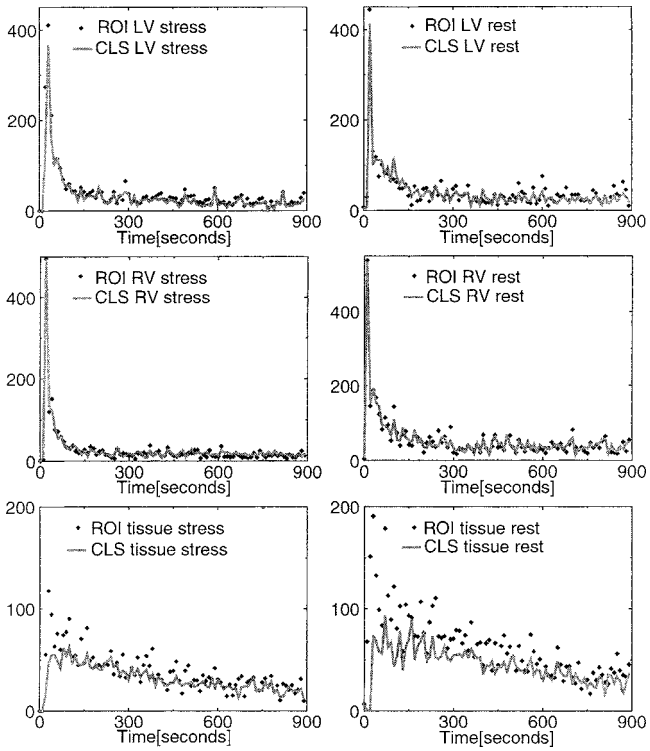

Figure 9. Results of the CLS method and ROI measurements for a patient teboroxime-99m stress study (first column) and rest study (second column). Rows correspond to LV, RV and myocardial tissue components.

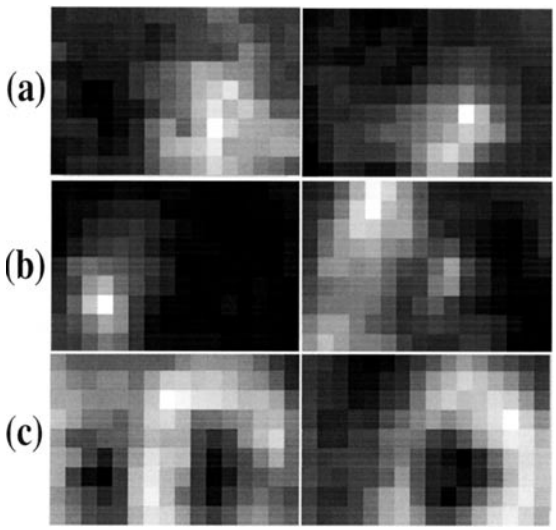

Figure 10. Images of factor coefficients obtained by the CLS method from patient data. The first column corresponds to the stress study and the second column corresponds to the rest study. Rows (a), (b) and (c) show coefficient images of LV, RV and myocardial tissue. In the images, the inferior part of the myocardium is missing: it was not taken into account due to liver contamination in the inferior area.

to the similarity of tissue curves and the large degree of noise in SPECT dynamic images. However, FADS is a useful tool for the automatic extraction of input functions from the LV and RV, which are at least as accurate as manual ROI measurements and have much better noise characteristics. Although the tissue curves may not be correct in abnormal studies, the image of tissue factor coefficients may serve as an indication of whether or not there is abnormality in the heart, and may aid in image segmentation.

The results of the CLS method were almost independent of the values of the weighting parameters (3), s_C and s_F, for $5000 > s_C, s_F > 100$. The absolute and relative values of these parameters affect the results of the LS method, but when the non-uniqueness correction is applied the results change to solutions which are very close to each other, regardless of the values of the parameters. The values of s_C and s_F used in this paper were 200 for the LS and CLS methods.

To determine the sensitivity of the results to the starting points, we performed FADS with different starting points for a given set of data. We found that if we started with reasonable starting points the results were not sensitive to the starting points. Reasonable starting points were determined by taking a constant value for the elements of the matrix **C**, and making the rows of the matrix **F** linearly independent. Also, the orders of magnitude of the elements in the matrix **CF** were chosen to agree with the order of magnitude of the analysed data. We found that when starting points were chosen randomly (random values of **C** and **F**) the algorithm sometimes failed to separate factors.

The LS method required a computationally expensive minimization procedure due to the non-linear objective function and the fairly large number of unknowns (the entries of **C** and **F**). No constraints, except non-negativity, were put on the values of **C** or **F**, but the algorithm was numerically stable for all the data used here. In terms of computation time, the calculation of a 20×19 pixel sub-region of a slice with 183 time frames took approximately 20 seconds on a SPARC Station 3000 (167 MHz) for the LS method and about 1 second for the AS method.

FADS with non-negativity constraints may lead to distinctly different solutions depending on the initial starting point, the FADS algorithm and the parameters of the algorithm. Even with all of those characteristics held constant, the difference can be substantial even for a different noise realization of the same numerical study. For the special case of teboroxime cardiac imaging it is possible to design a technique which can correct for these non-uniqueness effects, and, although the technique does not fully give unique answers (due to the unknown x_{TL} in (17)), FADS with correction for non-uniqueness provides a very good estimation of the input function and estimation of RV component, because the lack of knowledge of x_{TL} does not influence the LV and RV curves extracted by FADS.

Two distinct FADS methods were used for the extraction of factors and factor coefficients: the AS method described by Di Paola *et al* (1982) and the LS method described in section 2. The main difference between these two methods is the approach in the determination of the study subspace. In the AS method, the study subspace is determined by performing orthogonal analysis of the normalized vectors (normalized to 1) which represent changes of activity in each voxel. Oblique rotation is performed to impose non-negativity constraints. On the other hand, in the LS method, the study subspace is determined directly from the data and the non-negativity constraints are simultaneously imposed on the solution so that the oblique rotation step, which is required in the AS method, is not needed here. Both approaches can be improved by taking into account the statistics of the data. Correspondence analysis can be implemented into the AS method as done by Benali *et al* (1993), and the objective function in the LS method can be modified to take into account the noise. However, both of these approaches require the knowledge of the variances of each voxel. These variances are typically unknown in reconstructed SPECT images. The estimation of these variances and their use in the FADS

methods will be an interesting continuation of the work presented in this paper. There does not appear to be any clear advantage or disadvantage of the AS method or LS method over the other. The LS approach enables easy incorporation of the priors such as the smoothness prior on the factors or factor coefficients, or of entropy (Sitek *et al* 1999a). The greatest disadvantage to the LS approach is that the number of factors in the image has to be known *a priori*. We found that the AS method performed similarly to the LS method, yet the results from both uncorrected methods were not accurate (table 1).

In our experience we found that the greatest disadvantage of FADS (both AS and LS) is its non-unique solution. The results of the LS and AS methods can differ greatly from each other due to non-uniqueness (tables 1, 2, figure 3). We demonstrated that FADS solutions with no correction for non-uniqueness do not give quantitatively correct results, and we had to implement *a priori* knowledge in order to make the solution quantitatively acceptable (table 2, figure 3).

A very important question is whether the assumptions made regarding *a priori* knowledge are correct. The computer simulations show that if these assumptions are correct, the method described in section 2.3 corrects for the non-uniqueness of FADS almost perfectly. However, in real studies these *a priori* assumptions are not completely valid because there will be some contribution from myocardial tissue in the LV and RV due to scatter and finite resolution so in fact $\tilde{\boldsymbol{C}}_T(\mathrm{RV}) \neq \mathbf{0}$ and $\tilde{\boldsymbol{C}}_T(\mathrm{LV}) \neq \mathbf{0}$. The error made in assuming that these equations are equal to zero is minimized by our method by automatic determination of the pixels in the RV and LV in which the tissue coefficients are the smallest. In so doing, the effects of scatter and finite resolution are minimized. Also, when large (volume) regions are taken into account in the FADS analysis, the error is smaller. This is because in volume data there are more available voxels among which *a priori* assumptions (a) and (b) from section 2.2 hold well. Assumptions (c) and (d) from section 2.2 hold very well since the high-amplitude voxels of the image RV coefficients are well separated spatially from the voxels with the highest amplitude in the LV so that the spillover between these two regions is minimal.

In cardiac imaging the presence of the liver is of concern, because it is positioned close to the heart and substantial uptake in the liver can bias the image. In all of the canine studies, the liver was held away from the heart with a bundle of gauze. Also, in all of the studies presented in this paper, the influence of the liver on the FADS results was minimized by not using the regions of the image where the liver was present. The disadvantage of this approach is that some useful information in the region of the liver is also rejected. The liver component can be included in the FADS analysis, and factor analysis can be performed successfully with a four-component image. However, the liver introduces an additional complication in terms of the correction for non-uniqueness. A similar approach to the one presented in this paper can be used with the liver component, but such an approach would require more *a priori* assumptions than were used in this study. We will consider this approach in future work. The development of a FADS approach that includes the liver might be extremely valuable clinically for patients in which the inferior wall is not diagnosable. That is, if the liver component is accurately identified, it can in theory be removed from the image. This could be done in static scans as well, as long as they were acquired dynamically.

6. Summary and conclusion

In this work, the use of factor analysis of dynamic structures for dynamic cardiac SPECT imaging was investigated by analysing computer simulations, experimental canine studies and patient studies.

The effects of non-uniqueness were studied with computer simulations and a method was designed to correct for the non-uniqueness of FADS for three-component cardiac imaging based on *a priori* knowledge. Corrected FADS were then applied to canine and patient studies. The LV, RV and tissue curves and images of curve coefficients were obtained. FADS-obtained curves that were corrected for non-uniqueness were compared to curves from ROI measurements and a strong agreement between them was established for LV and RV curves.

In their current state, the FADS methods developed here can be used as a semi-automatic method for robustly extracting accurate TACs from dynamic SPECT or PET images. The method is semi-automatic because it is still required that the operator specify the region in the image on which the factor analysis is to be performed. These methods may also be used as tools for segmentation which separates different components.

Acknowledgments

We thank the referees for their help in revising our manuscript. We also thank Gengsheng L Zeng, PhD, for his insightful comments and Sean Webb for carefully proof-reading the manuscript. The images presented in this paper were made using 'Specter' developed by Timothy Turkington, PhD.

This work was supported by NIH Grant No ROI HL 39792 and in part by the American Heart Association.

Appendix

The complete derivation of (16) is presented here. Evaluating (14) for the factor coefficients for the RV we have

$$\begin{aligned} \boldsymbol{C}_R(\mathrm{RV}) &= \tilde{\boldsymbol{C}}_R(\mathrm{RV}) \\ \boldsymbol{C}_L(\mathrm{RV}) &= x_{RL}\tilde{\boldsymbol{C}}_R(\mathrm{RV}) + \tilde{\boldsymbol{C}}_L(\mathrm{RV}) + x_{TL}\tilde{\boldsymbol{C}}_T(\mathrm{RV}) \\ \boldsymbol{C}_T(\mathrm{RV}) &= x_{RT}\tilde{\boldsymbol{C}}_R(\mathrm{RV}) + x_{LT}\tilde{\boldsymbol{C}}_L(\mathrm{RV}) + \tilde{\boldsymbol{C}}_T(\mathrm{RV}). \end{aligned} \tag{A1}$$

Using conditions (b) and (c) from (15)

$$\begin{aligned} \boldsymbol{C}_R(\mathrm{RV}) &= \tilde{\boldsymbol{C}}_R(\mathrm{RV}) \\ \boldsymbol{C}_L(\mathrm{RV}) &= x_{RL}\tilde{\boldsymbol{C}}_R(\mathrm{RV}) \\ \boldsymbol{C}_T(\mathrm{RV}) &= x_{RT}\tilde{\boldsymbol{C}}_R(\mathrm{RV}) \end{aligned} \tag{A2}$$

and dividing the second equation in (A2) by the first equation in (A2) we have that $x_{RL} = \boldsymbol{C}_L(\mathrm{RV})/\boldsymbol{C}_R(\mathrm{RV})$. Dividing the third equation in (A2) by the first equation in (A2) we obtain $x_{RT} = \boldsymbol{C}_T(\mathrm{RV})/\boldsymbol{C}_R(\mathrm{RV})$.

Using (14) we can also evaluate factor coefficients for the LV, and after imposing conditions (a) and (d) from (15) we have

$$\begin{aligned} \boldsymbol{C}_R(\mathrm{LV}) &= \mathbf{0} \\ \boldsymbol{C}_L(\mathrm{LV}) &= \tilde{\boldsymbol{C}}_L(\mathrm{LV}) \\ \boldsymbol{C}_T(\mathrm{LV}) &= x_{LT}\tilde{\boldsymbol{C}}_L(\mathrm{LV}). \end{aligned} \tag{A3}$$

Dividing the third equation in (A3) by the second equation in (A3) we obtain the value of $x_{LT} = \boldsymbol{C}_T(\mathrm{LV})/\boldsymbol{C}_L(\mathrm{LV})$.

Nothing can be gained from the consideration of the values of coefficients evaluated over the tissue component even assuming the additional *a priori* condition $\tilde{\boldsymbol{C}}_R(\mathrm{TI}) = \mathbf{0}$, because (14) takes the form

$$\begin{aligned} \boldsymbol{C}_R(\mathrm{TI}) &= \mathbf{0} \\ \boldsymbol{C}_L(\mathrm{TI}) &= \tilde{\boldsymbol{C}}_L(\mathrm{TI}) + x_{TL}\tilde{\boldsymbol{C}}_T(\mathrm{TI}) \\ \boldsymbol{C}_T(\mathrm{TI}) &= x_{LT}\tilde{\boldsymbol{C}}_L(\mathrm{TI}) + \tilde{\boldsymbol{C}}_T(\mathrm{TI}). \end{aligned} \tag{A4}$$

Equation (A4) is not solvable since $\tilde{\boldsymbol{C}}_L(\mathrm{TI})$, $\tilde{\boldsymbol{C}}_T(\mathrm{TI})$ and x_{TL} are unknown.

References

Barber D C 1980 The use of principal components in the quantitative analysis of gamma camera dynamic studies *Phys. Med. Biol.* **25** 283–92

Benali H, Buvat I, Frouin F, Bazin J P and Di Paola 1993 A statistical model for the determination of optical metric in factor analysis of medical image sequences (FAMIS) *Phys. Med. Biol.* **38** 1065–80

Brownlee K A 1965 *Statistical Theory and Methodology in Science and Engineering* (New York: Wiley) pp 295–6

Buvat I, Benali H, Frouin F, Bazin J P and Di Paola R 1993 Target apex-seeking in factor analysis on medical sequences *Phys. Med. Biol.* **38** 123–8

Cavailloles F, Bazin J P and Di Paola R 1984 Factor analysis in gated cardiac studies *J. Nucl. Med.* **25** 1067–79

Chiao P-C, Ficaro E P, Dayanikli F, Rogers W L and Schwaiger M 1994 Compartmental analysis of technetium-99m-teboroxime kinetics employing fast dynamic SPECT at rest and stress *J. Nucl. Med.* **35** 1265–73

Di Paola R, Bazin J P, Aubry F, Aurengo A, Cavailloles F, Herry Y and Kahn E 1982 Handling of dynamic sequences in nuclear medicine *IEEE Trans. Nucl. Sci.* **29** 1310–21

Huston A S 1984 The effect of apex-finding errors on factor images obtained from factor analysis and oblique transformation *Phys. Med. Biol.* **29** 1109–16

Houston A S and Sampson W F D 1997 A quantitative comparison of some FADS methods in renal dynamic studies using simulated and phantom data *Phys. Med. Biol.* **42** 199–217

Hudson H M and Larkin R S 1994 Accelerated image reconstruction using ordered subsets of projection data *IEEE Trans. Med. Imaging* **13** 601–9

Huesman R H and Mozoyer B M 1987 Kinetic data analysis with a noisy input function *Phys. Med. Biol.* **32** 1569–79

Nakamura M, Suzuki Y and Kobayashi S 1989 A method for recovering physiological components from dynamic radionuclide images using the maximum entropy principle: a numerical investigation *IEEE Trans. Biomed. Eng.* **36** 906–16

Nirjan K S and Barber D C 1985 Towards automatic analysis of dynamic radionuclide studies using principal components factor analysis *Phys. Med. Biol.* **30** 1315–25

——1986 Factor analysis of dynamic function studies using *a priori* physiological information *Phys. Med. Biol.* **31** 1107–17

Pedersen F, Bergstrom M, Bengtsson E and Langstrom B 1994 Principal component analysis of dynamic positron emission tomography images *Eur. J. Nucl. Med.* **21** 1285–92

Press W H, Teukolsky S A, Vetterling W T and Flannery B P 1996 *Numerical Recipes in C* (Cambridge: Cambridge University Press) pp 420–5

Shepp L A and Vardi Y 1982 Maximum likelihood reconstruction for emission tomography *IEEE Trans. Med. Imaging* **1** 113–22

Sitek A, Di Bella E V R and Gullberg G T 1999a Factor analysis of dynamic structures in dynamic SPECT using maximum entropy *Trans. Nucl. Sci.* **46** 2227–32

——1999b An improved factor analysis method for cardiac dynamic SPECT studies using *a priori* information *IEEE Nuclear Science Symp. Medical Imaging Conf. Record (October 24–30, 1999, Seattle, WA)* pp 1014–16

Smith A M, Gullberg G T and Christian P E 1996 Experimental verification of technetium 99m-labelled teboroxime parameters in the myocardium with dynamic single-photon emission computed tomography: reproducibility, correlation to flow, and susceptibility to extravascular contamination *J. Nucl. Cardiol.* **3** 130–42

Smith A M, Gullberg G T, Christian P E and Datz F L 1994 Kinetic modelling of teboroxime using dynamic SPECT imaging of a canine model *J. Nucl. Med.* **35** 484–95

Tsui B M W, Terry J A and Gullberg G T 1993 Evaluation of cardiac cone-beam SPECT using observer performance experiments and ROC analysis *Inv. Radiol.* **28** 1101–12

Wu H-M, Hoh C K, Choi Y, Schelbert H R, Hawkins R A, Phelps M E and Huang S C 1995 Factor analysis for extraction of blood time–activity curves in dynamic FDG-PET studies *J. Nucl. Med.* **36** 1714–22